Excellent thermoelectric performance of ZrTe2 thin films and device

Chun Hung Suen
Hong Kong Polytechnic University
Songhua Cai
Nanjing University
Hui Li
The Hong Kong University of Science and Technology
Long Zhang
College of Physics, Chongqing University
Kunya Yang
College of Physics, Chongqing University
Huichao Wang
Peking University
Mingquan He
College of Physics, Chongqing University
Yisheng Chai
Chongqing University https://orcid.org/0000-0003-0034-7488
Kai Zhou
College of Physics, Chongqing University
Chi Man Wong
The Hong Kong Polytechnic University
Jiannong Wang
Hong Kong University of Science and Technology https://orcid.org/0000-0002-6133-6371
Xiaoyuan Zhou
Chongqing University
Jiyan Dai (jiyan.dai@polyu.edu.hk)
Hong Kong Polytechnic University https://orcid.org/0000-0002-7720-8032

Article

Keywords: Thermoelectric, ZrTe2 thin film, high mobility, interface, transition metal dichalcogenides

Posted Date: January 11th, 2021

DOI: https://doi.org/10.21203/rs.3.rs-141752/v1

Excellent thermoelectric performance of $ZrTe_2$ thin films and device

Chun Hung Suen[1+], S.H. Cai[1+], H. Li[2+], Long Zhang[3], Kunya Yang[3], Huichao Wang[4,], M.Q. He[3], Y.S. Chai[3], K. Zhou[3], Chi Man Wong[1], J.N. Wang,[2,*] X. Y. Zhou[3,*] and Ji-Yan Dai[1,*]*

[1] Department of Applied Physics, The Hong Kong Polytechnic University, Hung Hom, Kowloon, Hong Kong, China

[2] Department of Physics, Hong Kong University of Science and Technology, Hong Kong, China

[3] College of Physics, Chongqing University, Chongqing 401331, China

[4]School of Physics, Sun Yat-sen University, Guangzhou 510275, China

Abstract

Achieving high thermoelectric power factor in thin film heterostructures is essential for integrated and miniatured thermoelectric device applications. In this work, we demonstrate a mechanism and device performance of enhanced thermoelectric power factor through coupling the interfacial confined two-dimensional electron gas (2DEG) with thin film conductivity in a transition metal dichalcogenides-$SrTiO_3$ heterostructure. Owing to the formed conductive interface with two-dimensional electron confinement effect and the elevated conductivity, the $ZrTe_2/SrTiO_3$ (STO) heterostructure presents enormous thermoelectric power factor as high as $4 \times 10^5\ \mu W cm^{-1}K^{-2}$ at 20 K and $4800\ \mu W cm^{-1}K^{-2}$ at room temperature. Formation of quasi-two-dimensional electrons gas at the interface is attributed to the giant Seebeck coefficient, and enhanced electrical conductivity is suggested to be originated from charge transfer induced doping in the $ZrTe_2$, which leads to extremely large thermoelectric power factor. By taking the thermal conductivity of STO substrate as a reference, the effective zT value of this heterostructure can reach 1.5 at 300 K. This high thermoelectric figure of merit is demonstrated by a prototype device based on this heterostructure which results in 3K temperature cooling by passing through a current of 100 mA. This superior thermoelectric property makes this heterostructure a promising candidate for future thermoelectric device, and more importantly, paves a new pathway to design promising high-performance thermoelectric systems.

Keywords: Thermoelectric; $ZrTe_2$ thin film; high mobility; interface; transition metal dichalcogenides

[+] These authors contribute equally

[*]corresponding contact:

Jiyan.dai@polyu.edu.hk; xiaoyuan2013@cqu.edu.cn; songhua.cai@polyu.edu.hk; phjwang@ust.hk

Introduction

High-performance thermoelectric thin films have been attracting growing interests as a hot topic in condensed matter physics and materials science recently[1-3]. The development of micro-cooling devices and miniaturized self-powered devices are technically important for improvement of large-scale integrated circuits, which drives the study of thin film thermoelectric. For example, in microprocessors, the "hot spot" regions with higher power density frequently cause the fatal thermal failure. Therefore, thin film-based thermoelectric device becomes a potential solution for in-demand cooling of circuits. Furthermore, high-performance thermoelectric thin films are also essential to build micro-power generators for self-powered devices in environments where a thermal gradient exists; this is significant for power engineering and management in future electronics.

The performance of thermoelectric material can be evaluated by a dimensionless figure of merit $zT = S^2\sigma T/(\kappa_e + \kappa_l)$, where S, σ, T, κ_e, κ_l represent Seebeck coefficient, electrical conductivity, absolute temperature, electronic thermal conductivity and lattice thermal conductivity, respectively[4,5]. To enhance the figure of merit, numerous efforts have been devoted to improve the power factor (power factor = $S^2\sigma$)[6-10] or reduce the thermal conductivity[11-15]. Among those methods to realize large thermoelectric power factor in thin film/substrate, interface engineering has been proven to be an effective approach to enhance Seebeck effect of the heterostructure. Especially, the presence of quasi-two-dimensional electron gas (quasi-2DEGs) at the interface provides a dominant contribution to the enhancement of |S|[1,16-19]. As an ideal substrate with unique structure, physical and chemical properties, $SrTiO_3$ (STO) has been widely applied in thin film growth as well as the exploration of novel low-dimensional physics[1,20-25]. For example, the unique electronic phenomena generated from the heterointerface between epitaxial oxide layer and the STO substrate such as the very intriguing $LaAlO_3/SrTiO_3$ system has raised much attention. However, although the LAO/STO interface generally shows enhanced |S|, itself has not been found to exhibit an outstanding thermoelectric power factor for meaningful applications mainly due to the limitation on its electrical conductivity. For designing of available high-performance thermoelectric system, it is necessary to couple both high electrical conductivity and the enhanced thermoelectricity on a single heterointerface.

Here, we demonstrate the realization of giant thermoelectric power factor in $ZrTe_2/SrTiO_3$ heterostructure, which mainly attribute to the coupling between interfacial quasi-2DEG generated in STO substrate and the high conductivity of transition metal dichalcogenides (TMDs) film. An interfacial reaction between the pulsed-laser deposition (PLD) deposited layered $ZrTe_2$ thin film and STO substrate leads to the appearance of quasi-2DEG which enhancing the Seebeck coefficient. Meanwhile, the conductivity is also dramatically enhanced which may contribute from the doping effect of TMD film induced by charge transfer. Combining both the high Seebeck coefficient and electrical conductivity, this heterostructure system eventually presents an outstanding thermal power factor as well as thermoelectric figure of merit zT value, which is further demonstrated in a cooling

device. This work provides a promising pathway for designing of high-performance thermoelectric systems and opens new possibilities for exploration and development of intriguing thermoelectric materials, structures as well as thin film-based electronic devices.

Methods

In this study, PLD was used to grow $ZrTe_2$ films using an alloy target with Zr:Te=1:5; and insulating (100) STO was selected as the substrate. The substrate-target distance during the deposition was 5 cm, with the base pressure of around 5×10^{-5} Pa, and the films were grown at optimized substrate temperature (T_s) of 550 ℃. To preserve the $ZrTe_2$ film from oxidation in air, an additional AlN capping layer was deposited on the top of $ZrTe_2$ film at 200 ℃. The laser source was a KrF excimer laser with a wavelength of 248 nm. Different thicknesses of $ZrTe_2$ films from 5 nm to 10 nm, 35 nm and 60 nm were deposited on STO substrate and the AlN capping layer is about 70 nm with amorphous structure.

X-ray Diffraction (XRD) with Cu Kα_1 source was used to determine the orientation and crystalline phase of $ZrTe_2$ film. To determine the microstructure and thickness of $ZrTe_2$ film, transmission electron microscope (TEM) was used for cross-sectional characterization. High-resolution TEM (HRTEM) images were acquired on JEOL 2100F TEM, operated at 200 kV. Scanning TEM (STEM) images were acquired on Thermofisher Titan G2 60-300 aberration corrected S/TEM. The accelerating voltage of electron beam is 300kV. The convergence angle of electron probe for STEM-HAADF imaging is 22.5 mrad and the collection angle of annular detector is 79.5-200 mrad. A Gatan dual-EELS system was used for STEM-EELS data acquisition. For EELS line scan, the acquisition time per pixel is 1 s. The acquisition energy range is 420 to 720 eV with 0.1 eV dispersion, including the major or minor edges of oxygen and Ti.A 9T-PPMS (Physical Properties Measurement System) was utilized for measuring the Seebeck coefficient and electrical conductivity at a temperature range from 2 K to 300 K. The measurement of Seebeck coefficient and electrical conductivity in the range from 300 K to 600 K was carried out on Joule Yacht MRS-3 thin film thermoelectric parameter test system. The thermoelectric cooling experiments were conducted using a home-built setup. To make a good electrical contact, a layer of Au stripes across the sample width were deposited on $ZrTe_2$ thin film directly followed by the AlN capping layer. Then silver epoxy was used to connect gold contacts with current source leads after removing AlN on top of gold stripes while keeping the rest part of sample protected. The total contact resistance of both terminals is about 10 Ω. Two Pt-100 thermometers were used to record temperatures on both sides. The current was applied using a Keithley 6221 AC/DC current source.

Results and discussion

The fine structure of as-grown samples is directly related to their performances, so the microstructure and composition of all samples were firstly investigated. Figure 1(a) shows the cross-sectional High-resolution TEM (HRTEM) image of the $ZrTe_2$ film and STO substrate. One can see that the layer-structured $ZrTe_2$ occupies the major part of the deposited film, presenting clear (0001) lattice fringes

parallel to the substrate. This result is consistent to the layered structure of $ZrTe_2$ as shown in the schematic in Figure 1(b). $ZrTe_2$ has a hexagonal close-packed crystal structure, with space group of $P\bar{3}m1$. A stable 1T (trigonal) $ZrTe_2$ phase has an octahedral coordination of metal atoms[26] that can be illustrated as a CdI_2-type structure[27]. A unit cell of $ZrTe_2$ is denoted by a cyan rectangle in Figure 1(b) and can also be identified in the magnified high-resolution TEM (HRTEM) image. The crystal structure of our $ZrTe_2$ film was also characterized by XRD. Figure 1(c) presents the XRD pattern of the sample with 60 nm-thick film, where peaks at 2θ = 13.3 °, 26.9 °, 40.8 ° and 55.4 ° correspond to the *c*-axis (0001), (0002), (0003) and (0004) diffraction peaks of hexagonal $ZrTe_2$ (a = 0.395 nm, c = 0.663 nm, JCPDS #54-560), respectively. These results imply that the $ZrTe_2$ film is preferentially grown along *c*-axis, which is also consistent to the layer-by-layer characteristic observed in TEM. However, it should be pointed out that, besides the *c*-axis orientation, other orientation peaks can also be found in the film, suggesting that the $ZrTe_2$ film growth is not epitaxial.

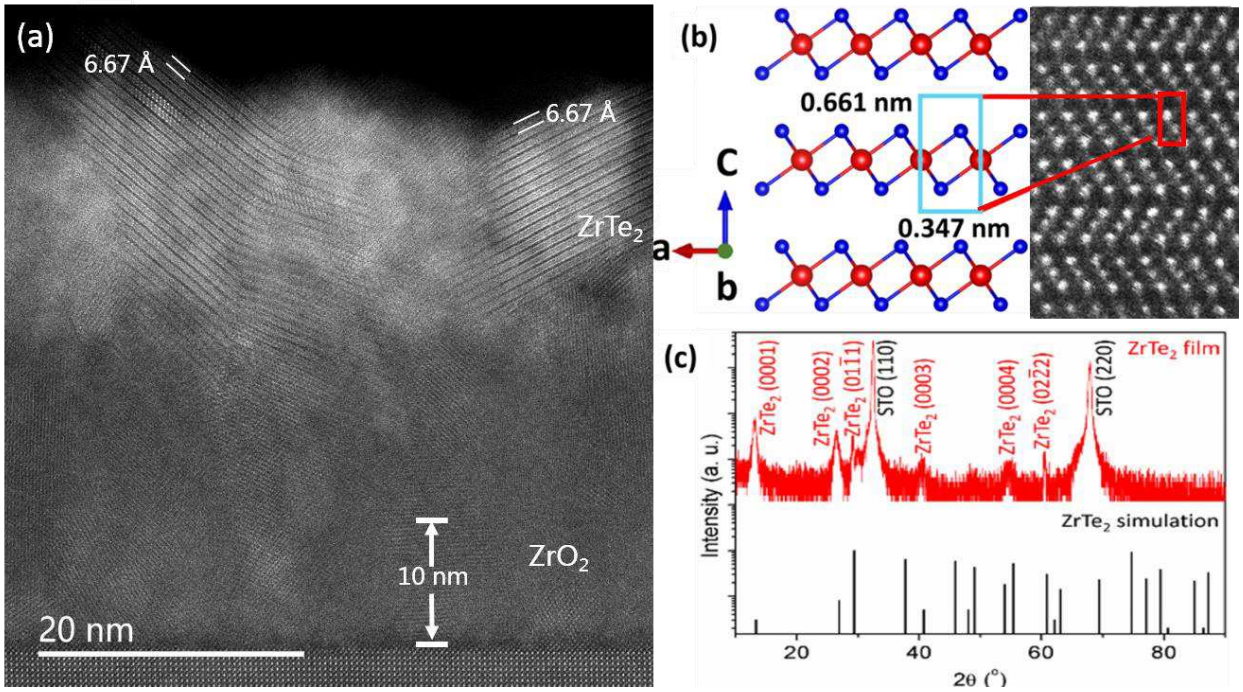

Figure 1 Crystal structure characterization (a) High-resolution TEM image of the $ZrTe_2$ film on STO substrate, where an interfacial layer of ZrO_2 reaction phase can be identified between the STO substrate and the $ZrTe_2$ film. (b) Magnified image of yellow rectangle region in (a) showing the correspondence of real unit cell with the crystal structure model of $ZrTe_2$. The unit cell is denoted by a rectangle to compared with magnified high-resolution TEM image of the $ZrTe_2$ film. (c) Typical XRD patterns of the $ZrTe_2$ films. The $ZrTe_2$ simulation pattern (JCPDS #54-560) is also illustrated for comparison.

It is worth noting that between the layered $ZrTe_2$ and the STO substrate, there exists a ~10 nm thick interfacial layer with different lattice structure with $ZrTe_2$. A detailed analysis of the lattice spacings

and their angles suggests that this interfacial layer belongs to ZrO_2 (See Figure S1). This implies that interfacial reaction occurs between the deposited $ZrTe_2$ and the STO substrate, and the interfacial characteristic has remarkably influenced the physical properties of both $ZrTe_2$ and the STO substrate. This can be revealed by the STEM energy disperse x-ray (EDX) spectroscopy element mapping and the electron energy loss spectroscopy (EELS) analysis of the interfacial region as shown in Figure 2. It is apparent in EDX mapping results shown in Figure 2(a), that the distributions of O and Te are not uniform along the thickness direction, i.e., the signal intensity of Te increases near the interface with a decrease of O signal. It is surprise to see that O even exists in the whole film, suggesting an out diffusion of O from STO which can be proven by EELS line-scan analysis across the interface as shown in Figure 2(b) and (c). By extracting the signals of Ti and O edges from the EELS spectrum, the energy loss near edge structures (ELNES) reveals that the 4 unit cells of STO from interface exhibits a different chemical state with bulk STO. From the 4th layer of STO up to the interfacial layer, the valence state of Ti cations degrades from Ti^{4+} to Ti^{3+} (peak shift and shape variation in Figure 2(b) with a corresponding change of O k-edge fine structure (Figure 2(c)). The interfacial characteristics imply a conductive STO surface, which analogous to the similar situation in the oxide heterostructures such as LAO/STO cases.

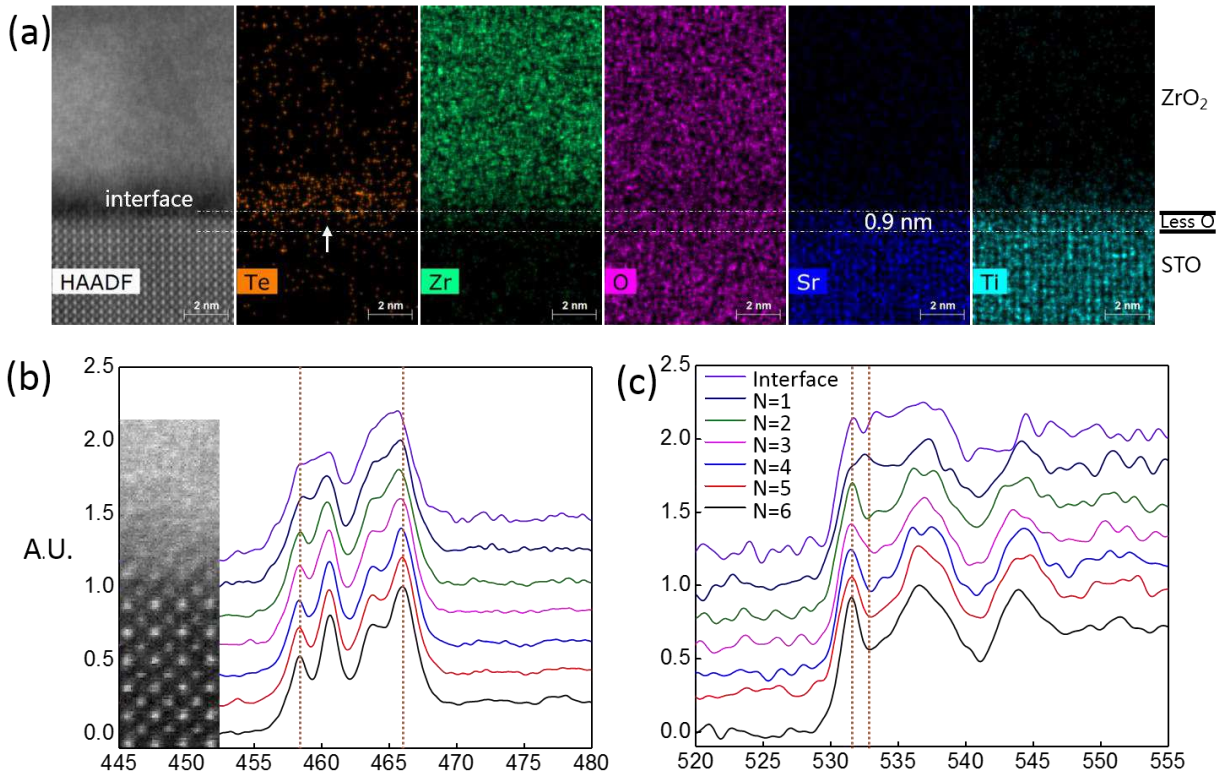

Figure 2 Elemental mapping and interfacial valence states of Ti and O ions (a) STEM-EDS element mapping across the interface, (b) EELS results of Ti 3d-L edge shift peaks, and (c) O -2p K edge fine structure across the interface.

We have carried out thermoelectric and electron transport properties measurements to different thicknesses of samples at temperatures ranging from 2K to 600K. The $ZrTe_2$/STO heterostructures exhibit negative Seebeck coefficient throughout the whole temperature range, indicating a n-type conducting characteristic; and the general trend is that the thicker films show relatively lower Seebeck coefficient but with high conductivity, while very thin films present highly fluctuated Seebeck coefficient and high resistance. Figure 3(a) shows the temperature-dependent Seebeck coefficients of the $ZrTe_2$/STO heterostructure with the 35 nm and 60 nm $ZrTe_2$ films from 2 K to 600 K. The Seebeck coefficient in the sample with a 35 nm-thick $ZrTe_2$ generally increases with the temperature increases from 2 K and finally reaches the maximum value of about 530 μV/K at 440 K, above which the Seebeck coefficient begins to decrease. The sample with 60 nm-thick $ZrTe_2$ film shows a similar trend while the maximum Seebeck coefficient appears at 111 K with a value of 368 μV/K. The temperature-dependent electrical conductivity of both samples are shown in Figure 3(b), which confirms that these heterostructures are highly conductive. The electrical conductivity can reach a remarkable value up to 10^7 S/cm at low temperature state (2 K). The coexistence of both very large Seebeck coefficient and high electrical conductivity of the $ZrTe_2$/STO heterostructure consequently leads to enormous thermoelectric power factor. As shown in Figure 3(c), the thermoelectric power factors monotonically increase with the decreasing of temperature in both samples and finally achieve a colossal value even exceeds $3 \times 10^5\ \mu W cm^{-1} K^{-2}$ at 20 K.

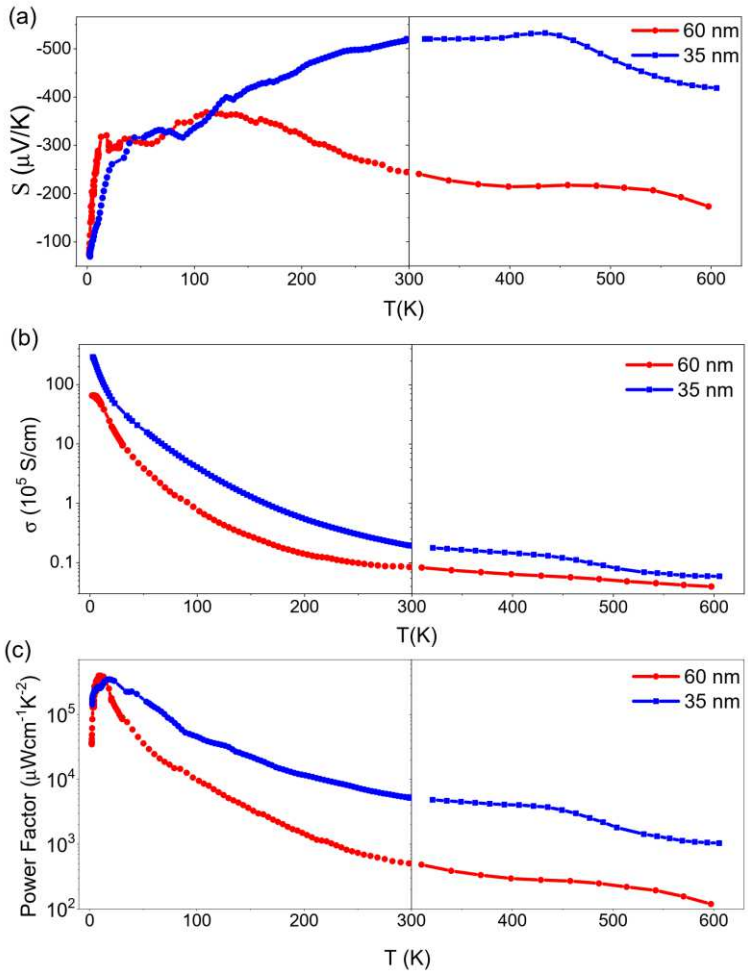

Figure 3 Thermoelectric and electrical conductive properties Temperature-dependent thermoelectric properties of the $ZrTe_2$/STO heterostructures with 35 nm and 60 nm-thick $ZrTe_2$ film in the temperature range of 2-600 K. (a) Seebeck coefficient, (b) electrical conductivity, and (c) thermoelectric power factor.

As well known, quasi-2DEG can exist in the conductive STO interface and its presence can be a prime factor for triggering intriguing thermoelectric properties. To clarify the contribution of the possible interfacial effect to the outstanding thermoelectric properties, we further conducted systematic electron transport measurements on the heterostructure. Compared to our previous work[26], the sample's quality has been further improved by optimizing the growth parameters. In these high quality heterostructures, we observed obvious Shubnikov–de Haas (SdH) oscillations superimposed on the large magnetoresistance at low temperatures below 4 K. Figure 4(a) shows the oscillations after subtracting a smooth background from the measured magnetoresistance of a typical 60 nm-thick $ZrTe_2$ film on STO. The periodicity in the reciprocal of magnetic field (1/B) demonstrates the SdH effect is the origin. Fast Fourier Transform (FFT) results further reveal that the oscillating frequency peak is about 29.5 T as shown in Figure 4(b). By analyzing the temperature dependence of the oscillations using the Lifshitz-Kosevitch formula, we obtain an effective mass of $1.3m_0$ with m_0 represents the bare electron

mass (Figure 4(c)). In addition, the Dingle temperature is calculated as 1.4 K based on the measured quantum oscillations. It is interesting to find that the microscopic parameters of the quantum oscillations actually agree well with those acquired in conductive STO surfaces[28-35]. Thus, we believe that the interfacial effect between the $ZrTe_2$ thin film and the STO substrate plays a significant role for presenting the very exotic transport properties in our observation[26].

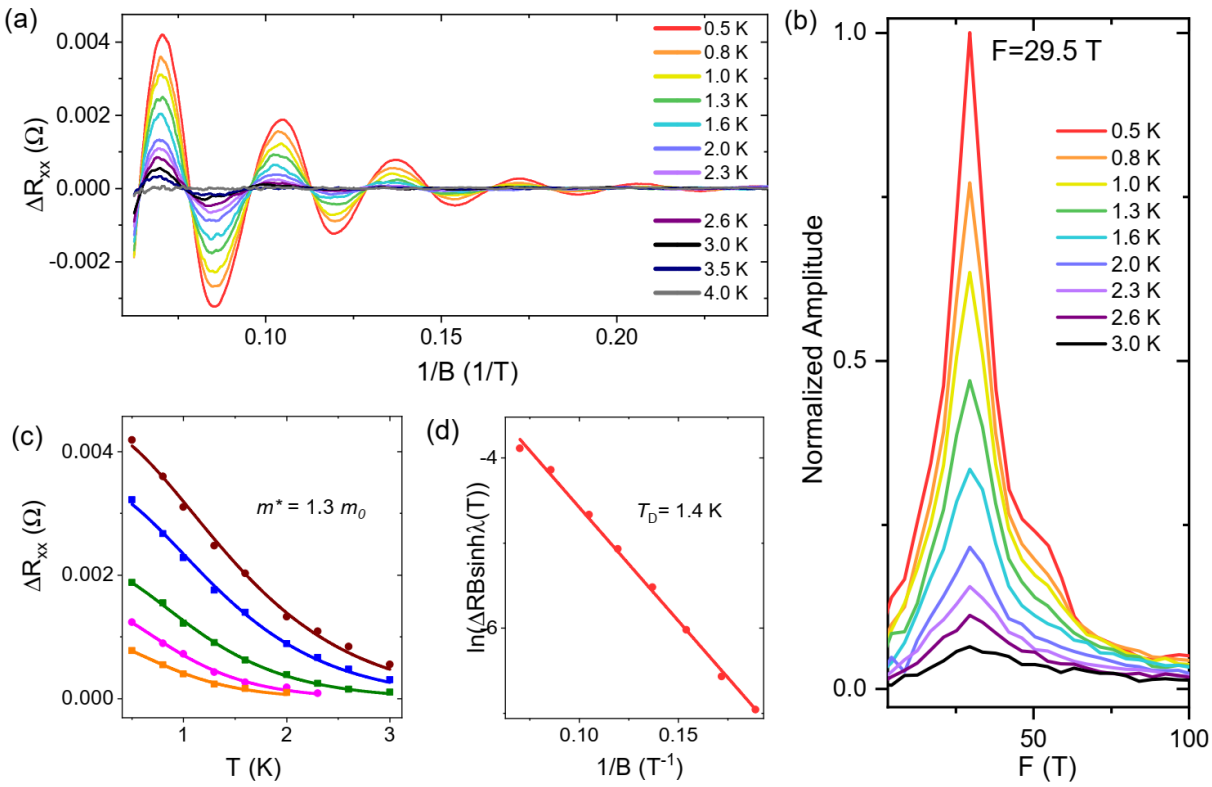

Figure 4 Quasi two-dimensional transport characteristic of the heterostructure (a) SdH quantum oscillations in the $ZrTe_2$/STO, and (b) FFT results of the oscillations revealing a frequency peak of 29.5 T. (c) and (d) are calculated effective mass and Dingle temperature based on the Lifshitz-Kosevitch formula.

Our previous study on the $ZrTe_2$/STO heterostructures has revealed a quasi-2D transport characteristic of the hybrid heterostructure, within which the electrons exhibit a high mobility of about $1.8 \times 10^4\ cm^2V^{-1}s^{-1}$ at 2 K[26]. The quasi-2D transport feature is consistent to the layered structure of $ZrTe_2$ and the property of quasi-2D electrons in the STO interface as well. These characteristics are supposed to be responsible for the observed enormous Seebeck coefficient and power factor. Similar findings also exist in TiO_2/STO, LAO/STO and FeSe/STO heterostructures[1,36,37]. In the TiO_2/STO heterostructure, with the presence of 2DEG, the room temperature (300 K) Seebeck coefficient is as large as 1050 $\mu V/K$; while our $ZrTe_2$/STO heterostructures show a value of $|S|_{300K}$ smaller than 500 $\mu V/K$ (Figure 3(a)). It is worth noting that the Seebeck coefficient of the heterostructure shows

obvious dependency with the thickness of the TMD film that a thicker $ZrTe_2$ film will lead to the decrease of |S|. Figure S shows comparison of our results to reported Seebeck coefficients from other 2D systems. In fact, a control sample with only the interfacial contribution from ZrO_2/STO shows much higher Seebeck coefficient with a value of about 750 μV/K at 300 K, well consistent with the result in the TiO_2/STO heterostructure[1] (See Figure S3) . Meanwhile, the electric conductivity is also found to be thickness dependent; while this dependence is opposite to that of the Seebeck coefficient. The control sample with only ZrO_2/STO shows a much higher resistance, making the Seebeck coefficient measurement fluctuate vigorously and also prevents the system achieving a higher power factor. As a conclusion, the deposition of TMD $ZrTe_2$ thin films on the top of the quasi-2D system induces slight decrease of the Seebeck coefficient of the system due to its relatively lower Seebeck coefficient, but it contributes very high conductivity to the system. With the coupling between the thin $ZrTe_2$ film and the STO-based interface, the largest thermoelectric power factor can be achieved in the $ZrTe_2$/STO heterostructure with an optimized thickness.

However, it should be noted that if at a much thinner thickness, the interface is not well conductive and EELS results show that the valence state of Ti cations at the interfacial region is still Ti^{4+} instead of Ti^{3+} (see **Error! Reference source not found.**). Therefore, we come to the conclusion that the interfacial state for forming a confined 2D conductive interface is essential for achieving the outstanding thermoelectric properties in this system. On the other hand, the extremely high conductivity is another crucial factor for realization of the giant thermopower factor. We also prepare a $ZrTe_2$ thin film on the insulating Al_2O_3 (Figure S) to clarify the origin. It can be found that the $ZrTe_2$ thin film is indeed metallic with a high conductivity but still lower than the value achieved in the $ZrTe_2$/STO system, this also suggests a modulation effect to the $ZrTe_2$ film from the interface. As a reference, the FeSe/STO is a well-explored metal/STO heterostructure system due to the interface-enhanced high temperature superconductivity [38,39]. Strong evidences have shown that the interfacial electron-phonon coupling as well as the electron doping on the FeSe layer should be responsible for the high temperature superconductivity of the FeSe/STO system[40-44]. In particular, the electron doping to the film through the thermal annealing generally decreases the resistance of the system and thus enhances the conductivity[45]. We suggest that similar mechanism may also exist in the metallic $ZrTe_2$/STO heterostructure that the electron doping from the substrate to the TMD film determines the very high conductivity of the system. More efforts are needed to further demonstrate the underlying physical origins.

It is noticeable that there exists a small peak in the Seebeck coefficient at about 20 K (Figure 3(a)), and this can be explained by the phonon-drag effect[46-48] originated from the STO (100) substrate. One study that related to the thermal transport of STO[49] exhibits a thermal conductivity peak close to 20 K. When a thermal gradient is applied to the thin film and substrate, nonequilibrium phonons will be generated and transfer their momentum to the carriers; as a result, an additional electric field is formed

in the film, thus enhance the Seebeck coefficient. The characteristic of phonon-drag effect is that, it is more effective at temperatures where the substrate attains its maximum thermal conductivity; this is the reason why the peak of Seebeck coefficient, as shown in Figure 3(a), is near the temperature where the substrate exhibits its peak thermal conductivity.

For thin films, the substrate thermal conductivity dominated the thermal transport, so we estimate the effective thermoelectric figure of merit zT is mainly based on the value of thermoelectric power factors of the film and the reported thermal conductivity values of STO single crystal[50]. For the 35 nm $ZrTe_2$/STO sample, the zT value at 300 K is about 15, which is extremely higher compared to all reported works according to the best our knowledge. Even for the 60 nm thick $ZrTe_2$ film sample, zT is about 1.5 at 300 K and increases to 13 at 18 K.

The superior thermoelectric performance of our $ZrTe_2/SrTiO_3$ heterostructure is further demonstrated by thermoelectric cooling experiments as shown in Figure 5 at room temperature of $T_{hot-side}$=300 K and ambient atmosphere. The Peltier effect allows the heat to be pumped from the cold end towards the hot-side (heat sink) by applying positive currents due the n-type nature of our device. As shown in Figure 5(a), clear asymmetric temperature difference $\Delta T = T_{cold-side} - T_{hot-side}$ produced by Peltier effect is seen by reversing current directions although Joule heating dominants at currents above 20 mA. This Joule heating is inevitable as the total resistance of the device is about 20 Ω including ~10 Ω of sample resistance and ~10 Ω of contact resistance. Nevertheless, the Joule heating is overcome at positive current of 20 mA and a net temperature difference of -0.15±0.05 K is achieved. To visualize the intrinsic Peltier cooling, the Joule effect is subtracted out in Fig.5 (b) as $\Delta T_{\text{Peltier}} = 1/2(\Delta T_{I+} - \Delta T_{I-})$ assuming a symmetric response of Joule heating. Noticeable cooling about 3 K is achieved even using a moderate current I=100 mA for a $ZrTe_2$(60 nm)/$SrTiO_3$ standalone device. Measurements using current in the Amperes region were not successful due to extremely high current density load to the nanometer scale thin film. Nevertheless, the cooling effect is in comparable to that of commercial Bi_2Te_3 devices in the small current and linear response region as presented by inset in Fig.5(b). Note that such a Kelvin level temperature difference is produced only by a nanometer scale thermoelectric working unit loaded with millimeter-sized substrate, if incorporating with a p-type leg, it could reduce the heat load significantly, and likely push the temperature difference to a much higher level.

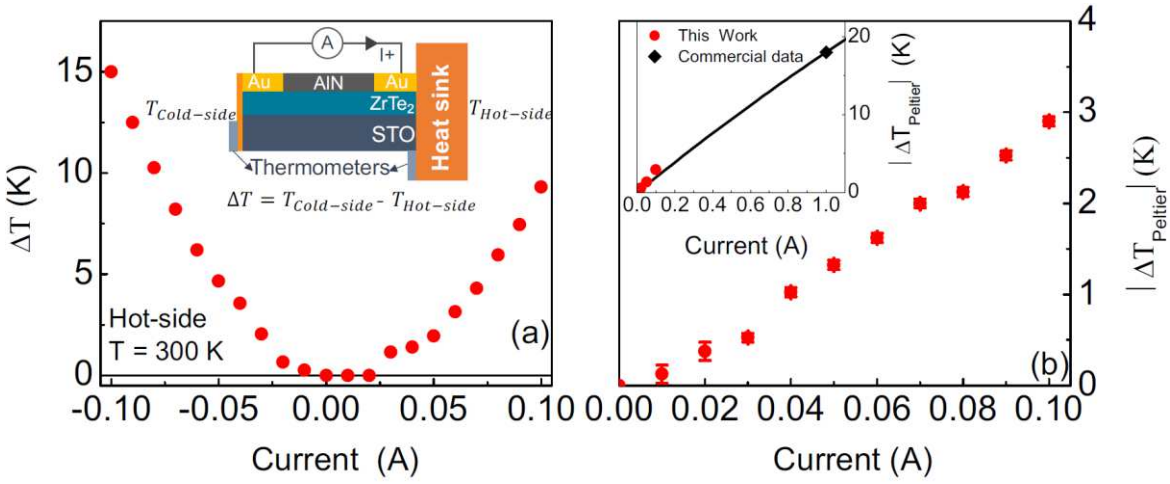

Figure 5 Thermoelectric cooling performances. (a) Net temperature difference $\Delta T = T_{cold-side} - T_{hot-side}$ produced by a $ZrTe_2$(60 nm)/$SrTiO_3$ device using varies currents. (b) Peltier cooling $\Delta T_{\text{Peltier}} = 1/2(\Delta T_{I+} - \Delta T_{I-})$ evaluated after subtracting the Joule heating by symmetrizing the direct temperature differences at opposite currents shown in (a). The inset in (a) shows a schematic setup used for thermoelectric cooling test. The inset in (b) compares the Peltier cooling of our device to that of a Bi_2Te_3 based commercial device.

Conclusion

In summary, we demonstrate that the $ZrTe_2$/STO heterostructure possesses colossal thermoelectric power factor at both low temperature and room temperature which has been further demonstrated in a cooling device. The excellent thermoelectric properties can be attributed to the formation of two-dimensional electrical transport property as well as the enhanced conductivity due to charge transfer occurs in the interface. This study reveals the promising thermoelectric properties of $ZrTe_2$/STO heterostructure and provides a new pathway for development of thermoelectric materials and structures. Furthermore, the mechanism exploration is of fundamental importance for both thermoelectric physics and possible application on thin film-based electronic devices.

Acknowledgements

We thank support from The Hong Kong Polytechnic University (Grant Nos. 1-ZVCG, 1–ZVGH, 4–ZZDC, and DD7F). X. Zhou acknowledges financial support from National Natural Science Foundation of China (NSFC) (Grant No. 11674040, 11904039) and the Fundamental Research Funds for the Central Universities (Grant no. 2018CDQYWL0048, 106112017CDJQJ308821 and 2018CDPTCG0001/26). H.W. acknowledges the support of the Hundreds of Talents program of Sun Yat-Sen University and the Fundamental Research Funds for the Central Universities (No. 20lgpy165).

Supporting Information for

Enormous thermoelectric power factor of $ZrTe_2/SrTiO_3$ heterostructure

Chun Hung Suen[1+], S.H. Cai[1+], H. Li[2+], Long Zhang[3], Kunya Yang[3], Huichao Wang[4,], M.Q. He[3], Y.S. Chai[3], K. Zhou[3], Chi Man Wong[1], J.N. Wang,[2,*] X. Y. Zhou[3,*] and Ji-Yan Dai[1,*]*

[1] Department of Applied Physics, The Hong Kong Polytechnic University, Hung Hom, Kowloon, Hong Kong, China

[2] Department of Physics, Hong Kong University of Science and Technology, Hong Kong, China

[3] College of Physics, Chongqing University, Chongqing 401331, China

[4] School of Physics, Sun Yat-sen University, Guangzhou 510275, China

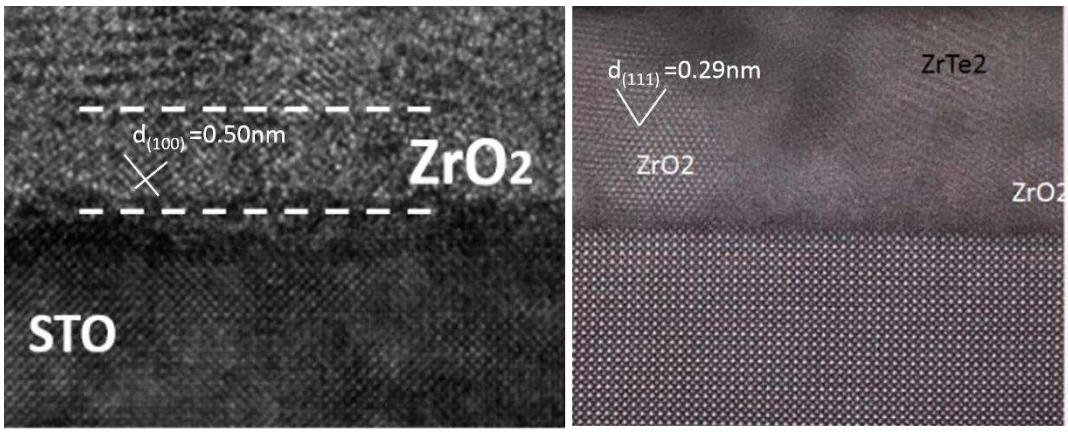

Figure S1. (a) HRTEM and (b) STEM image of the interfacial structure. ZrO_2 becomes the dominant component near the interface area.

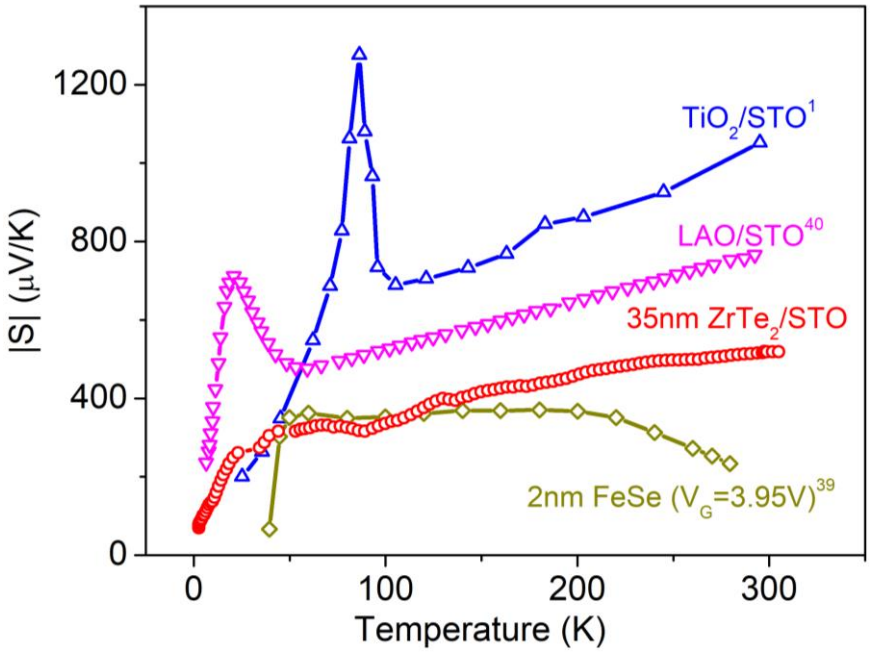

Figure S2. Comparison of temperature dependent Seebeck coefficient among 2D systems.

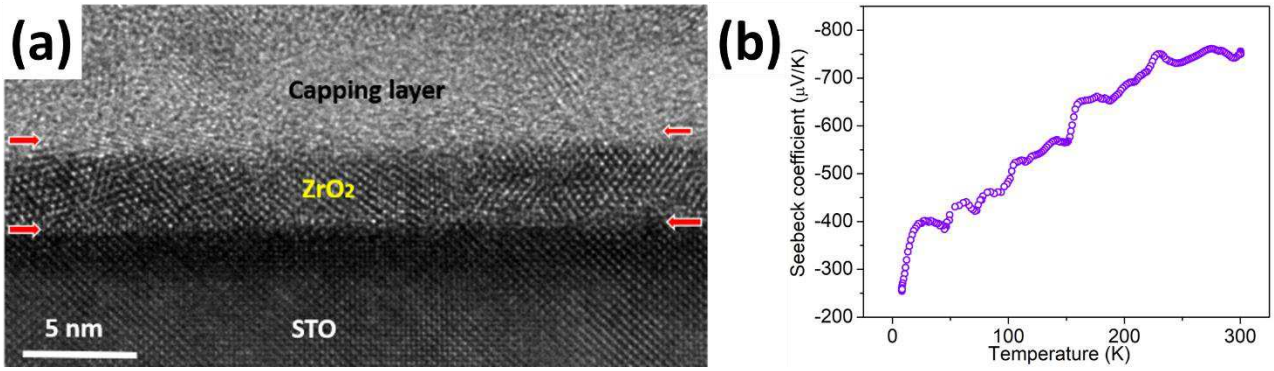

Figure S3. (a) HRTEM image of the thinnest control sample (5nm ZrO_2/STO), and (b) the Seebeck coefficient showing that the control sample has much a higher value but unstable due to its high resistance.

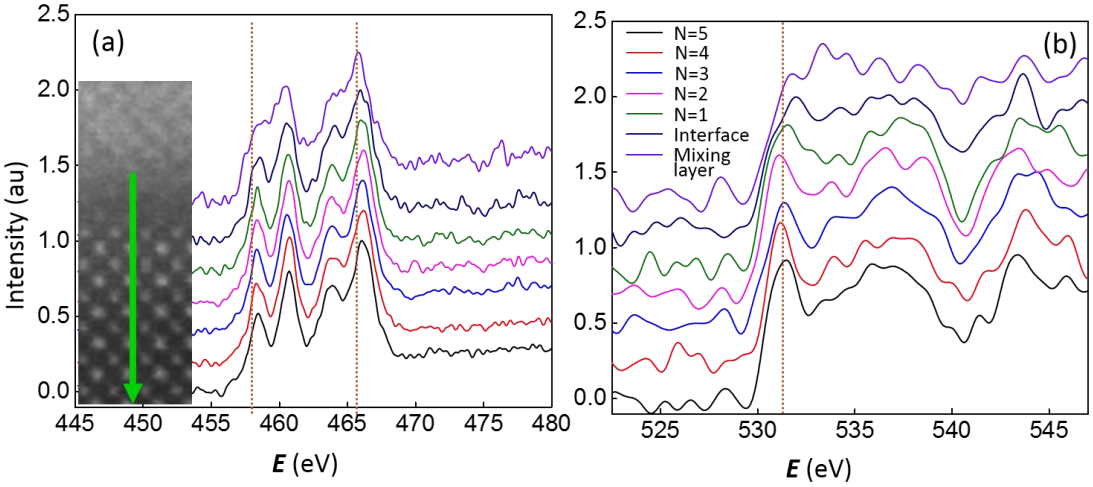

Figure S4 Elemental mapping and interfacial valence states of Ti and O ions (a) STEM-EDS element mapping across the interface, (b) EELS results of Ti 3d-L edge shift peaks, and (c) O -2p K edge fine structure across the interface.

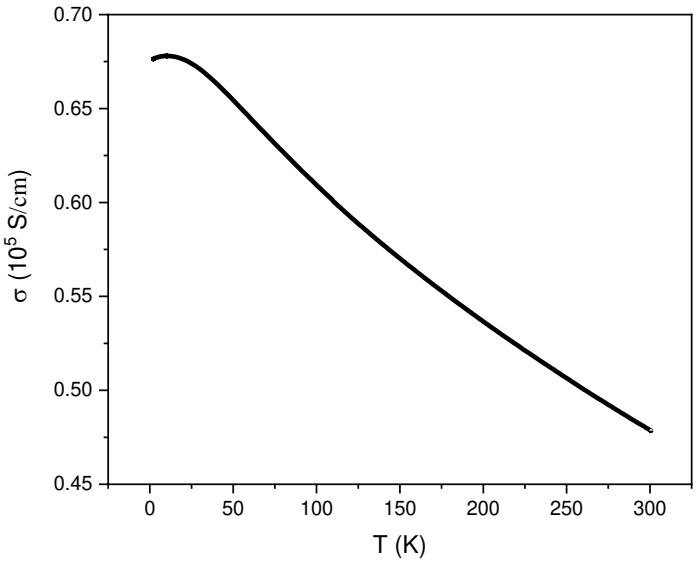

Figure S5. Conductivity-temperature relationship in the $ZrTe_2$ thin films on Al_2O_3 substrate.

References

1 Ohta, H. *et al.* Giant thermoelectric Seebeck coefficient of a two-dimensional electron gas in $SrTiO_3$. *Nat Mater* **6**, 129-134 (2007).

2 Rama, V., Edward, S., Thomas, C. & Brooks, O. Q. Thin-film thermoelectric devices with high room-temperature figures of merit. *Nature* **413**, 597-602 (2001).

3 Chen, X., Zhou, Z., Lin, Y.-H. & Nan, C. Thermoelectric thin films: Promising strategies and related mechanism on boosting energy conversion performance. *Journal of Materiomics* **6**, 494-512 (2020).

4 Altenkirch, E. Uber den Nutzeffeckt der Thermosaule. *Physikalische Zeitschrifr* **10** (1909).

5 Altenkirch, E. Electrothermische Kalteerzeugung and Reversible Electrische Heizung. *Physikalische Zeitschrifr* **12**, 920 (1911).

6 Hicks, L. D. & Dresselhaus, M. S. Effect of quantum-well structures on the thermoelectric figure of merit. *Physical Review B* **47**, 12727-12731 (1993).

7 Heremans, J. P. *et al.* Enhancement of Thermoelectric Efficiency in PbTe by Distortion of the Electronic Density of States. *Science* **321**, 554-557 (2008).

8 Pei, Y. *et al.* Convergence of electronic bands for high performance bulk thermoelectrics. *Nature* **473**, 66-69 (2011).

9 Liu, W. *et al.* Convergence of conduction bands as a means of enhancing thermoelectric performance of n-type $Mg_2Si_{1-x}Sn_x$ solid solutions. *Phys. Rev. Lett.* **108**, 166601 (2012).

10 Suen, C. H. *et al.* Enhanced thermoelectric properties of SnSe thin films grown by pulsed laser glancing-angle deposition. *Journal of Materiomics* **3**, 293-298 (2017).

11 Biswas, K. *et al.* High-performance bulk thermoelectrics with all-scale hierarchical architectures. *Nature* **489**, 414-418 (2012).

12 Hsu, K. F. *et al.* Cubic $AgPb_mSbTe_{2+m}$: Bulk Thermoelectric Materials with High Figure of Merit. *Science* **303**, 818-821 (2004).

13 Zhao, L.-D. *et al.* Ultralow thermal conductivity and high thermoelectric figure of merit in SnSe crystals. *Nature* **508**, 373-377 (2014).

14 Peng, K. *et al.* Broad temperature plateau for high ZTs in heavily doped p-type SnSe single crystals. *Energy & Environmental Science* **9**, 454-460 (2016).

15 Liu, H. *et al.* Copper ion liquid-like thermoelectrics. *Nat. Mater.* **11**, 422-425 (2012).

16 Nagase, K., Takado, S. & Nakahara, K. Thermoelectric enhancement in the two-dimensional electron gas of AlGaN/GaN heterostructures. *physica status solidi (a)* **213**, 1088-1092 (2016).

17 Ohta, H., Kim, S. W., Kaneki, S., Yamamoto, A. & Hashizume, T. High Thermoelectric Power Factor of High-Mobility 2D Electron Gas. *Adv Sci (Weinh)* **5**, 1700696 (2018).

18 Rhyee, J. S. *et al.* Peierls distortion as a route to high thermoelectric performance in $In_4Se_{3-\delta}$ crystals. *Nature* **459**, 965-968 (2009).

19 Fukutani, K., Sato, T., Galiy, P. V., Sugawara, K. & Takahashi, T. Tunable two-dimensional

electron gas at the surface of thermoelectric material In_4Se_3. *Physical Review B* **93**, 205156 (2016).

20 Ohtomo, A. & Hwang, H. Y. A high-mobility electron gas at the $LaAlO_3/SrTiO_3$ heterointerface. *Nature* **427**, 423-426 (2004).

21 Reyren, N. *et al.* Superconducting Interfaces Between Insulating Oxides. *Science* **317**, 1196-1199 (2007).

22 Gabay, M. & Triscone, J.-M. Hund rules with a twist. *Nature Physics* **9**, 610-611 (2013).

23 Dikin, D. A. *et al.* Coexistence of superconductivity and ferromagnetism in two dimensions. *Phys Rev Lett* **107**, 056802 (2011).

24 Ben Shalom, M., Sachs, M., Rakhmilevitch, D., Palevski, A. & Dagan, Y. Tuning spin-orbit coupling and superconductivity at the $SrTiO_3/LaAlO_3$ interface: a magnetotransport study. *Phys Rev Lett* **104**, 126802 (2010).

25 Caviglia, A. D. *et al.* Tunable Rashba spin-orbit interaction at oxide interfaces. *Phys Rev Lett* **104**, 126803 (2010).

26 Wang, H., Chan, C. H., Suen, C. H., Lau, S. P. & Dai, J. Y. Magnetotransport Properties of Layered Topological Material $ZrTe_2$ Thin Film. *ACS Nano* **13**, 6008-6016 (2019).

27 Machado, A. J. S. *et al.* Evidence for topological behavior in superconducting Cu_xZrTe_{2-y}. *Physical Review B* **95**, 144505 (2017).

28 Kozuka, Y. *et al.* Two-dimensional normal-state quantum oscillations in a superconducting heterostructure. *Nature* **462**, 487-490 (2009).

29 Chen, Y. Z. *et al.* A high-mobility two-dimensional electron gas at the spinel/perovskite interface of γ-$Al_2O_3/SrTiO_3$. *Nat Commun* **4**, 1371 (2013).

30 Ben Shalom, M., Ron, A., Palevski, A. & Dagan, Y. Shubnikov-de Haas oscillations in $SrTiO_3/LaAlO_3$ interface. *Phys Rev Lett* **105**, 206401 (2010).

31 Yang, M. *et al.* High field magneto-transport in two-dimensional electron gas $LaAlO_3/SrTiO_3$. *Applied Physics Letters* **109** (2016).

32 McCollam, A. *et al.* Quantum oscillations and subband properties of the two-dimensional electron gas at the $LaAlO_3/SrTiO_3$ interface. *APL Materials* **2** (2014).

33 Rubi, K. *et al.* Aperiodic quantum oscillations in the two-dimensional electron gas at the $LaAlO_3/SrTiO_3$ interface. *npj Quantum Materials* **5** (2020).

34 Lin, X. *et al.* Critical Doping for the Onset of a Two-Band Superconducting Ground State in $SrTiO_{3-\delta}$. *Physical Review Letters* **112** (2014).

35 Caviglia, A. D. *et al.* Two-dimensional quantum oscillations of the conductance at $LaAlO_3/SrTiO_3$ interfaces. *Phys Rev Lett* **105**, 236802 (2010).

36 Shimizu, S. *et al.* Giant thermoelectric power factor in ultrathin FeSe superconductor. *Nat. Commun.* **10**, 825 (2019).

37 Pallecchi, I. *et al.* Giant oscillating thermopower at oxide interfaces. *Nat Commun* **6**, 6678 (2015).

38 Wang, Q.-Y. *et al.* Interface-Induced High-Temperature Superconductivity in Single Unit-Cell FeSe Films on $SrTiO_3$. *Chinese Physics Letters* **29** (2012).
39 Zhang, W.-H. *et al.* Direct Observation of High-Temperature Superconductivity in One-Unit-Cell FeSe Films. *Chinese Physics Letters* **31** (2014).
40 Tang, C. *et al.* Interface-enhanced electron-phonon coupling and high-temperature superconductivity in potassium-coated ultrathin FeSe films on$SrTiO_3$. *Physical Review B* **93** (2016).
41 Song, C. L. *et al.* Observation of Double-Dome Superconductivity in Potassium-Doped FeSe Thin Films. *Phys Rev Lett* **116**, 157001 (2016).
42 Zhang, W. H. *et al.* Effects of Surface Electron Doping and Substrate on the Superconductivity of Epitaxial FeSe Films. *Nano Lett* **16**, 1969-1973 (2016).
43 Zhang, H. *et al.* Origin of charge transfer and enhanced electron-phonon coupling in single unit-cell FeSe films on $SrTiO_3$. *Nat Commun* **8**, 214 (2017).
44 Zhao, W. *et al.* Direct imaging of electron transfer and its influence on superconducting pairing at FeSe/$SrTiO_3$ interface. *Sci. Adv.* **4** (2018).
45 Wang, Q. *et al.* Thickness dependence of superconductivity and superconductor–insulator transition in ultrathin FeSe films on $SrTiO_3$ (001) substrate. *2D Materials* **2** (2015).
46 Fletcher, R., Zaremba, E. & Zeitler, U. *Electron-Phonon Interactions in Low-Dimensional Structures*. Chap. 5 (Oxford University Press, 2003).
47 Gallagher, B. L. & Bucher, P. N. *Handbook on Semiconductors*. Vol. 1 817 (Elsevier, 1992).
48 Wang, G., Endicott, L., Chi, H., Lost'ak, P. & Uher, C. Tuning the temperature domain of phonon drag in thin films by the choice of substrate. *Phys. Rev. Lett.* **111**, 046803 (2013).
49 Martelli, V., Jimenez, J. L., Continentino, M., Baggio-Saitovitch, E. & Behnia, K. Thermal transport and phonon hydrodynamics in strontium titanate. *Phys. Rev. Lett.* **120** (2018).
50 Valentina, M., Julio, L. J., Mucio, C., Elisa, B. S. & B., K. Thermal transport and phonon hydrodynamics in strontium titanate. *Phys Rev Lett* **120**, 125901 (2018).
51 Hurd, C. M. *The hall effect in metals and alloys*. (Springer, 1972).
52 Morozova, N. V., Korobeinikov, I. V., Kurochka, K. V., Titov, A. N. & Ovsyannikov, S. V. Thermoelectric Properties of Compressed Titanium and Zirconium Trichalcogenides. *The Journal of Physical Chemistry C* **122**, 14362-14372 (2018).
53 Hippalgaonkar, K. *et al.* High thermoelectric power factor in two-dimensional crystals of MoS_2. *Physical Review B* **95** (2017).

Figures

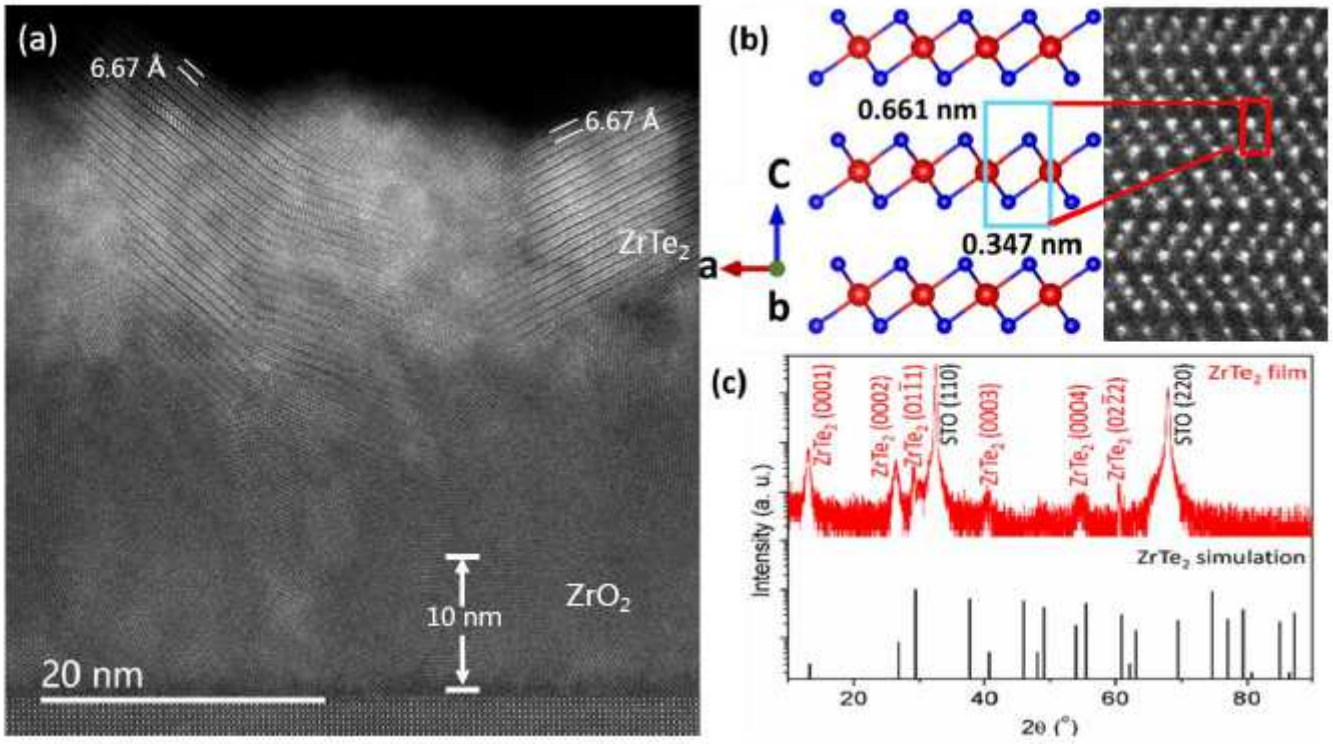

Figure 1

Crystal structure characterization (a) High-resolution TEM image of the ZrTe2 film on STO substrate, where an interfacial layer of ZrO2 reaction phase can be identified between the STO substrate and the ZrTe2 film. (b) Magnified image of yellow rectangle region in (a) showing the correspondence of real unit cell with the crystal structure model of ZrTe2. The unit cell is denoted by a rectangle to compared with magnified high-resolution TEM image of the ZrTe2 film. (c) Typical XRD patterns of the ZrTe2 films. The ZrTe2 simulation pattern (JCPDS #54-560) is also illustrated for comparison.

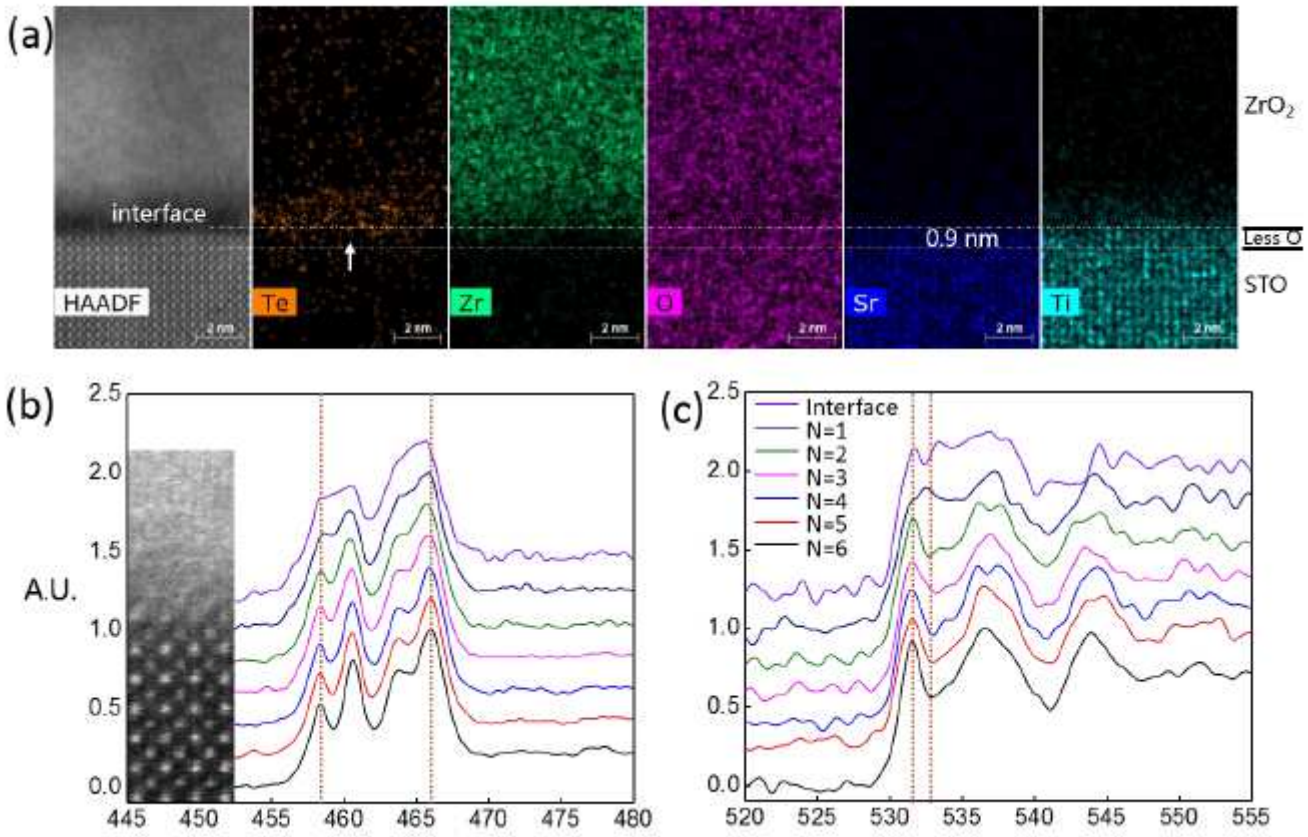

Figure 2

Elemental mapping and interfacial valence states of Ti and O ions (a) STEM-EDS element mapping across the interface, (b) EELS results of Ti 3d-L edge shift peaks, and (c) O -2p K edge fine structure across the interface.

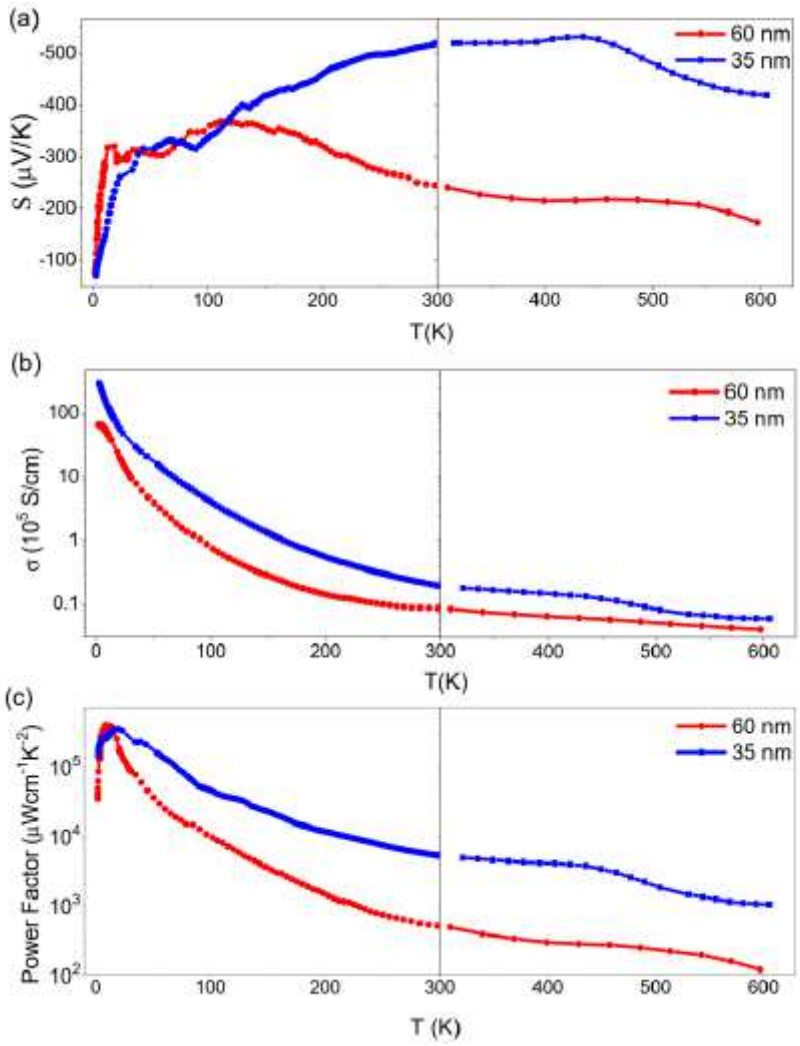

Figure 3

Thermoelectric and electrical conductive properties Temperature-dependent thermoelectric properties of the ZrTe2/STO heterostructures with 35 nm and 60 nm-thick ZrTe2 film in the temperature range of 2-600 K. (a) Seebeck coefficient, (b) electrical conductivity, and (c) thermoelectric power factor.

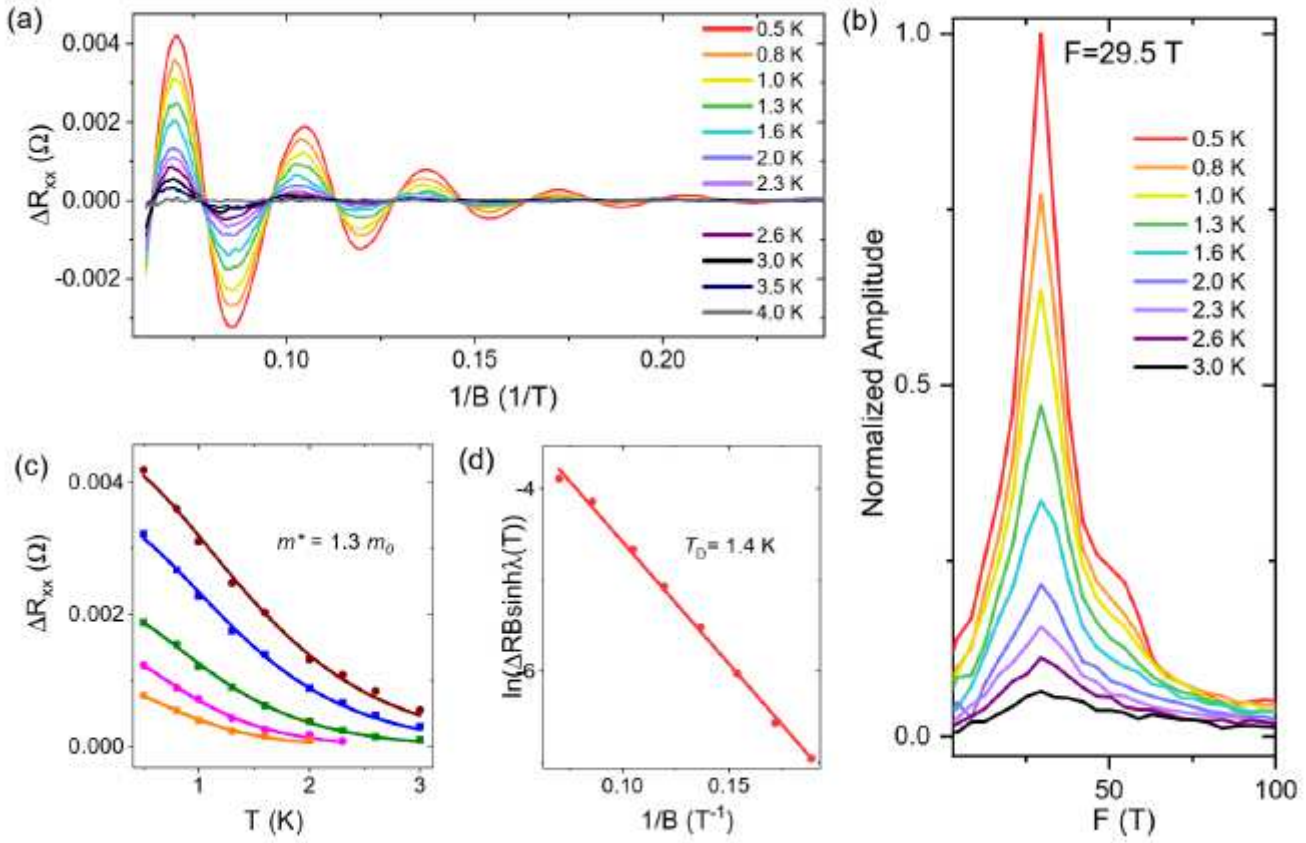

Figure 4

Quasi two-dimensional transport characteristic of the heterostructure (a) SdH quantum oscillations in the ZrTe2/STO, and (b) FFT results of the oscillations revealing a frequency peak of 29.5 T. (c) and (d) are calculated effective mass and Dingle temperature based on the Lifshitz-Kosevitch formula.

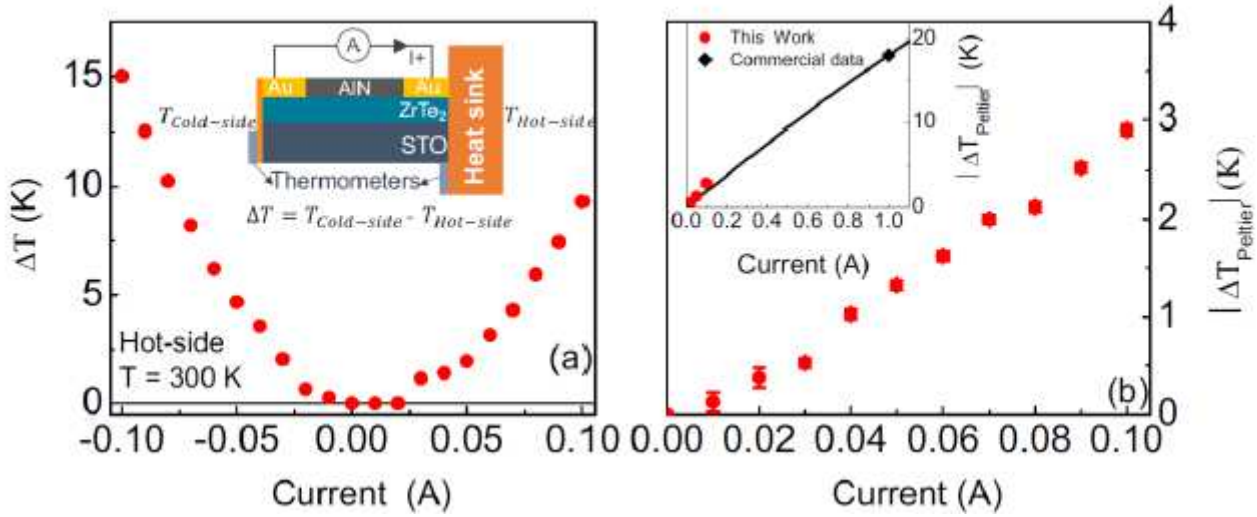

Figure 5

Thermoelectric cooling performances. (a) Net temperature difference Δ□=□□□□□−□□□□−□□□□−□□□□ produced by a ZrTe2(60 nm)/SrTiO3 device using varies currents. (b) Peltier cooling Δ□Peltier=1/2(Δ□□+−Δ□□−) evaluated after subtracting the Joule heating by symmetrizing the direct temperature differences at opposite currents shown in (a). The inset in (a) shows a schematic setup used for thermoelectric cooling test. The inset in (b) compares the Peltier cooling of our device to that of a Bi2Te3 based commercial device.